Food Hydrocolloids 123 (2022) 107001

Contents lists available at ScienceDirect

Food Hydrocolloids

journal homepage: www.elsevier.com/locate/foodhyd

Rheo-chemistry of gelation in aiyu (fig) jelly

Fan-Wei Wang [a], Michela Geri [b], Yun-Ju Chen [a], Jung-Ren Huang [a], Gareth H. McKinley [b,*], Yeng-Long Chen [a,c,**]

[a] Inst. Physics, Academia Sinica, Taipei, Taiwan
[b] Dept. Mechanical Engineering, Massachusetts Institute of Technology, Cambridge, MA, USA
[c] Physics Division, National Center for Theoretical Sciences, Taipei, Taiwan

ARTICLE INFO

Keywords:
Physical gelation
Methylesterase
Pectin gelation
Rheology
Cryo-SEM

ABSTRACT

We investigated the gelation characteristics of aiyu jelly derived from the polymeric extract obtained by washing the seeds of *Ficus Pumila* var. *Awkeotsang*. The main gel component is low methoxyl pectin, which forms crosslinks with divalent ions that bind the exuded polysaccharide chains. Unlike many fruit pectins used in jam and jellies that require heating, additional sugars, and acidic conditions to gel, the aiyu exudate gels at room temperature with just the addition of water. In this study, the time-resolved dynamics of the gelation process and the evolution of the viscoelastic relaxation spectrum with frequency and gel age are obtained via Optimally Windowed Chirp rheometry (OWCh), conventional time-sweep rheometry, and cryo-scanning electron microscope (cryo-SEM) microstructural characterization.

During gelation, we observed distinctive frequency-dependent inflection points in both the time-evolving storage and loss moduli which occur nearly simultaneously in time. Close inspection of high resolution cryo-SEM images taken at different times during the gelation process showed that the gels initially form nano-fiber networks with mesh sizes on the order of tens of microns and the stiffer mature gels observed at longer times develop sub-micron mesh sizes. These observations suggest a progressive transformation between microstructures may accompany the progressive growth in the elasticity of the aiyu gels and the local inflection points in the viscoelastic moduli.

We also developed a multi-species reaction kinetics model for calcium – pectin binding in aiyu gelation. By including methylesterase enzymatic conversion of pectin binding sites, combined with calcium binding and the slower formation of consecutively-bound junction zones, the distinctive inflection points in the viscoelastic moduli are captured by the kinetic gelation model. By combining rheological measurements, microstructural observations, and reaction kinetics modeling, this study not only characterizes a unique water-soluble natural extract that gels at room temperature with no additives or thermomechanical processing, it also demonstrates that the aiyu polysaccharide system is a safe and controllable model for gelation systems in which binding site activation is concurrently coupled to crosslink formation.

1. Introduction

The fig plant *Ficus Pumila* var. *Awkeotsang*, commonly known as aiyu, grows natively at 800m–2000m altitude in the hills of Taiwan. Due to the delicate ecological balance, aiyu production is very sensitive to shifting climates. Recent agricultural modifications have developed new varieties that grow at low altitudes to meet the shifting climates and large weather fluctuations (Wu et al., 2007). In 2018, approximately 700 tons of aiyu fig seeds were harvested in Taiwan (Lu et al., 2019). The mucilage extracted by washing the seeds of the pollinated aiyu fruit produces edible aiyu jelly that is served as a summer dessert. Unlike many pectin gels that require strong acidity and/or thermal activation to induce gelation (Gawkowska et al., 2018; Axelos et al., 1987; Chan et al., 2017), aiyu seeds need only rinsing in water to produce a pectin-rich solution that gels at room temperature (Huang et al., 1980; Oda & Tanaka, 1966; Suzuno et al., 1991, 1994). As such, this system is a naturally packaged food solution that produces a biodegradable and edible gel. The fruit, seeds, and jelly are shown in Fig. 1a. Aiyu jelly has

* Corresponding author.
** Corresponding author. Inst. Physics, Academia Sinica, Taipei, Taiwan.
E-mail addresses: gareth@mit.edu (G.H. McKinley), ylchen@gate.sinica.edu.tw (Y.-L. Chen).

https://doi.org/10.1016/j.foodhyd.2021.107001
Received 6 April 2021; Received in revised form 25 June 2021; Accepted 26 June 2021
Available online 2 July 2021

also been used for stomach ailments, weight and cholesterol control (Durand et al., 1990; Urias-Orona et al., 2010; Wang et al., 2019).

The physical properties of the gel produced can vary widely with the plant sub-variety and processing method. The maximum gel storage modulus can vary over two orders of magnitude, and the gelation time can vary by several hours. The softer jelly is often combined with sugary beverages, while firmer jelly is served with fruits and syrup. Currently, trial-and-error is used for grading the aiyu seeds for improving gel processing and properties. With physical characterization and fundamental understanding of the gelation mechanism, significant improvements in controlling the desired gel properties could be realized.

The active gelling ingredient in aiyu extract is poly-galacturonic acid (PGA), present in high amounts in the mucilage that is extracted by washing the seeds (Huang et al., 1980). PGA is also the active gelation agent in pectins extracted from fruits. The physical differences in the gel microstructure and stress response between various fruit pectins can be attributed to the PGA methyl ester side group content, which is designated as the *degree of methylation* (DM) (Chan et al., 2017; Durand et al., 1990; Jiang et al., 2001; Ngouemazong et al., 2012a). For high DM PGA, crosslinking between PGA chains occurs by hydrogen bonding and requires high temperature and low pH, such as used in common recipes for preparing fruit jams. For low DM PGA, the methyl ester side groups are cleaved by enzymatic action and converted to carboxylic acid. The carboxylic acids dissociate in water at pH between 5 and 6 and form ionic bonds with solvated ions. The reversible ion-PGA bond strength is comparable to thermal energy with frequent binding/unbinding events. The dynamic nature of this process is captured by an "egg-box model". The model proposes that divalent ions, often calcium, act as bridges and form consecutively bound stable nano-crystalline "egg-box" junction zones (denoted JZ henceforth) that crosslink solvated PGA chains (Durand et al., 1990; Garnier et al., 1993; Grant et al., 1973; Ventura et al., 2013). The JZ length in the calcium-pectin systems has been estimated to be greater than a critical length l_c that varies between $6 \leq l_c \leq 20$ consecutive bridging sites depending on the measurement method (Braccini & Pérez, 2001; Luzio & Cameron, 2008; Ventura et al., 2013).

The chemical composition of aiyu seed extract has been analyzed by inductively coupled plasma emission spectroscopy and other methods (Huang et al., 1980; Suzuno et al., 1997). Due to the variability of seeds and methodology, PGA content typically varies from 50 to 65 percent of the dry matter. Similarly, the methoxyl group weight content in PGA varies from 4 to 10%, with "high methoxyl" (HM) content designating > 7% by weight (and DM > 50%), and "low methoxyl" (LM) content < 7% (and DM < 50%). The extract also contains small amounts of inorganic elements (≈0.95 g Ca, 5 g K, 0.37 g Mg, and 0.35 g P in 100 g of dry matter) that are critical participants in forming a physical gel. Furthermore, Huang and coworkers identified pectin methylesterase enzyme in the extract that converts HM PGA to LM PGA, cleaving the methyl ester side group $-COOCH_3$ to form carboxylic acid groups –COOH, which progressively increases the number of binding sites for ions to bind PGA chains (Huang et al., 1980). The enzyme activity was found to be sensitive to temperature, pH, and NaCl concentration. Under normal conditions for preparation of aiyu gel (room temperature with tap water), the gelling process varies with the solution ion concentrations, PGA polymer content, and the ion-polymer binding strength. However, chemical composition analyses have not been shown to be quantitative predictors of physical gelation characteristics such as the gelation time and the gel modulus.

In this study, we report the physical characterizations of the mucilage extracted from one type of commercially purchased aiyu seeds. We examine how the extract dry weight and solution viscosity depend on the seed concentration. We also investigate how the gelation time and the maximum viscoelastic moduli of the mature gel evolve and depend

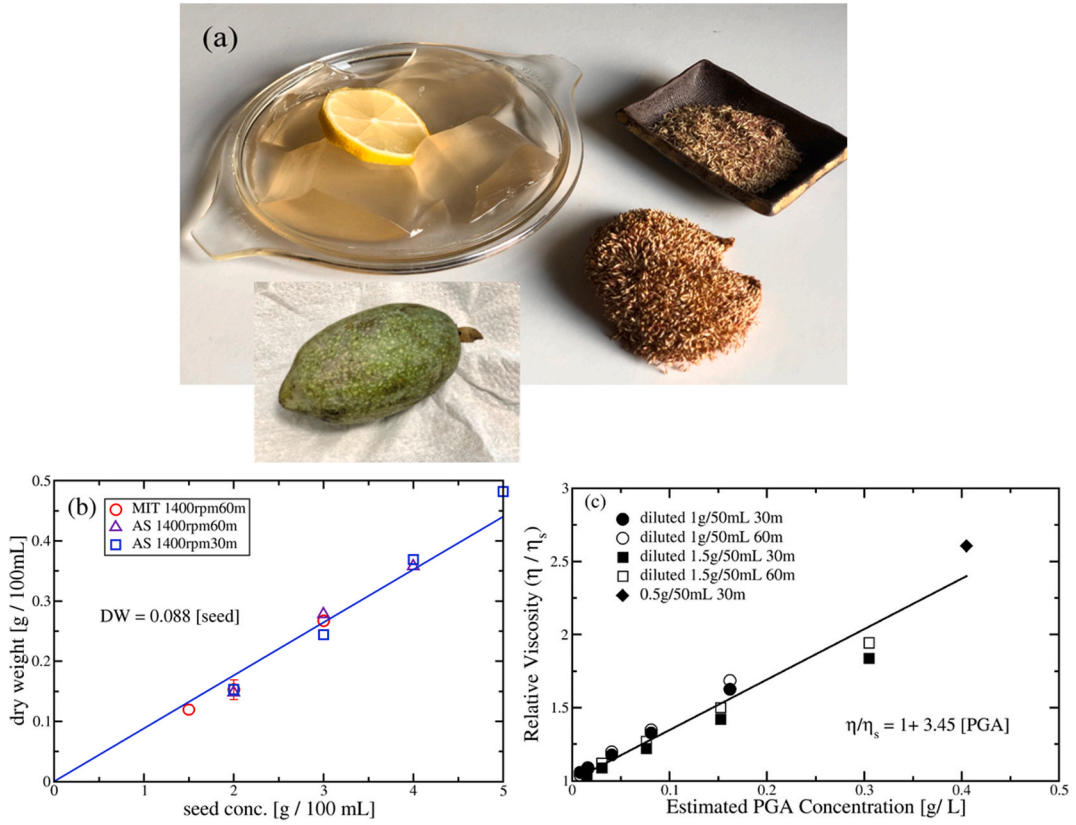

Fig. 1. (a) Counter clockwise from bottom left – a ripe aiyu fruit, an aiyu fruit that is turned inside out and dried, aiyu seeds, aiyu jelly with lemon; (b) Extract dry weight as function of the seed weight added to deionized water. The solid line is a linear fit with slope of 0.088; (c) Extract viscosity η relative to water (η_s) as a function of the estimated PGA concentration in the diluted extract. The solid line is a linear regression fit with slope of 3.45 L/g.

on NaCl and $CaCl_2$ concentrations. From these observations, we propose a gelation model based on established reaction kinetics to capture the unexpected trends observed in the temporal evolution of the viscoelastic moduli for the evolving aiyu gels.

2. Methods

The average sample weight of a single aiyu seed (obtained from Greenself Co, USA) was 2 ± 0.4 mg, measured by counting 324 seeds. Aiyu extracts were prepared by mixing seeds and deionized water (DI water, $> 10^6$ Ω-cm), with or without added NaCl and $CaCl_2$. The mixture was stirred at 1400 rpm for either 30 or 60 min, after which the seeds and the aqueous extract were separated. Approximately 20 mL of the extract was immediately loaded into the rheometer sample cup for rheometry measurements.

Another 15 mL of the extract was reserved for freeze drying to obtain the dry weight measurements. Aqueous aiyu extracts were placed in plastic tubes and flash frozen at −80 °C for 1 day. The tube was then pumped down to less than 70 Pa to dry by sublimation for one day. The freeze-sublimation process was repeated once more. As shown in Fig. 1, mixing 2.0 g of aiyu seeds in 100 mL DI water for 60 mins at 1400 rpm extracted 0.15 ± 0.01 g dry matter. For 3.0 g of aiyu seeds in 100 mL DI water, 0.26 ± 0.02 g dry matter was extracted. We assume approximately 60% of the dry matter is PGA based on prior composition analysis (Suzuno et al., 1997). There is very good agreement between samples prepared by mixing for 30 min and 60 min. The dried sample weight exhibits a linear dependence on the seed concentration and very little dependence on the mixing time. We thus expect a corresponding increase in the PGA and ion concentration with the mass concentration of seeds used to produce gels. The electrical conductivity (σ) of the extract from 3.0 g seeds in 100 mL DI water was found to be σ ≈ 500 μS/cm using a conductivity meter (Horiba Scientific). The conductivity also varied linearly with the seed concentration, indicating that the ratio of solvated ions to PGA chains remains constant.

The zero-shear rate viscosity of the aiyu extracts was measured with a capillary viscometer (Cannon-Fenske, size 50). Seed weights of 0.5 g, 1.0 g, and 1.5 g were mixed with 50 mL of DI water (conductivity < 1 μS/cm) and stirred at 1400 rpm for 30 mins or for 60 mins at 22 ± 1 °C. The extracts were subsequently diluted by factors of 5, 10, 20, 50, and 100 with DI water to prevent gelation during the viscometry measurements. We estimate the PGA weight in the diluted samples from the dry matter fraction as reported in Fig. 1b. The intrinsic viscosity $[\eta]$ of the diluted extract is approximately 3.45 L/g as determined from the slope of the best fitted line shown in Fig. 1c. We can also independently estimate the theoretical expected value of the intrinsic viscosity using the relationship (Graessley, 1980) $[\eta] = 0.77/c^*$, where $c^* = \overline{M_w}/(4/3\,\pi\,N_A\,R_g{}^3)$ is the coil overlap concentration and $\overline{M_w}$ is the average molecular weight, and N_A is Avogadro's number. The PGA molecular weight $\overline{M_w}$ is reported to be between 2 and 4 MDa, and the radius of gyration $R_g \approx$ 150 nm based on dynamic light scattering measurement (Suzuno et al., 1997). Using $\overline{M_w} = 2$ MDa, we calculate $c^* \approx 0.24$ g/L and $[\eta] = 0.77/c^* \approx 3.28$ L/g, which is in good agreement with the measured value. In addition, these values for aiyu molecular dimensions are consistent with another independent measurement (Axelos et al., 1987) that determined the PGA persistence length to be $l_p \approx 4.5$ nm. With a monomer galacturonic acid (GA) molecular weight of 194 Da, the degree of polymerization is $N_p \approx 10000$ (using $\overline{M_w} = 2$ MDa), and the estimated radius of gyration is $R_g \approx 180$ nm assuming an ideal random coil polymer conformation.

Optimally Windowed Chirp Rheometry (OWCh) measurements were conducted at the Hatsopoulos Microfluids Laboratory (MIT) with the TA ARES G2 rheometer using a concentric cylinder geometry (stainless steel, with bob diameter of 27.66 mm, cup diameter of 30 mm, and an operating distance of 3.6 mm above the base). The measurements were conducted at 22 ± 1 °C. Additional rheometry measurements were conducted at the Institute of Physics (AS) using the Anton-Paar MCR 301 rheometer with the CC-27 concentric cylinder geometry (stainless steel, with bob diameter of 26.66 mm, cup diameter of 28.92 mm, and an operating distance of 6.5 mm above bottom). Sample preparation followed the same procedures. For the experiments on the MCR 301, we performed time sweeps at a fixed oscillation frequency of $\omega = 10$ rad/s and 1% strain at 23 ± 1 °C, in the linear viscoelastic regime.

For the OWCh experiments, the following protocol was performed after the sample was loaded in the measuring cup: (a) a time sweep at a constant frequency of 10 rad/s and 1% strain until the storage modulus $G'(\omega, t)$ began to increase rapidly and approach the same order of magnitude as the viscous loss modulus $G''(\omega, t)$. (b) Short exponential chirps with frequency and amplitude modulation were then performed repeatedly until the time-evolving viscoelastic moduli approached their peak values. The OWCh method applies a windowed exponential chirp signal to the sample (Geri et al., 2018), with a frequency window range of $0.3 \leq \omega \leq 30$ rad/s that varies over a signal period of $\Delta t_{chirp} = 15$ s. (c) Finally, as the rate of sample mutation slowed in the mature gel, discrete frequency sweeps at intervals of approximately 30 min were again performed. As the gelation reaction during the seed washing process is unknown and hard to capture, we assume the reaction initiates from the very beginning of the washing process, using the total time as the time from the start of extraction, $t = (t_{stir} + t_{rheo})$, where the stirring time is t_{stir} and the rheometry observation time is t_{rheo}.

To observe microstructural evolution, aiyu extract was prepared and loaded for rheometry. At the same time, cryo-scanning electron microscopy (cryo-SEM) was performed (FEI ESEM Quanta 200, Thermo Fisher Scientific, US). A millimeter-sized droplet of aiyu extract was placed on a plastic membrane (PALL Corporation, US). The sample and the membrane were loaded onto a stage with Tissue-Tek® O.C.T. compound (Sakura Finetek, Japan) and swiftly frozen by soaking into liquid nitrogen for about 30 s. The sample was then placed in the vacuum chamber for sublimation at −75 °C for 25 min before imaging with SEM.

3. Results

3.1. PGA concentration affects gelation time and moduli

We anticipate that increasing the number of washed seeds per unit volume will increase the extracted PGA concentration, with significant consequences for the subsequent gelation characteristics. As shown in Fig. 2a, the gelation onset appears progressively earlier as the seed concentration is increased. In this study, we identify a good estimate for the gel point t_{gel} to be the time at which the storage and loss moduli are equal, i.e. $G'(\omega, t) = G''(\omega, t)$, rather than the time at which the phase angle $\tan(\delta) = G''/G'$ is constant for all ω. Due to the small initial magnitudes of both G' and G'' (≈0.01–0.1 Pa), individual measurements can fluctuate significantly, and we are able to more accurately interpolate the data to find the time at which $G' = G''$.

As the seed concentration increases from 1.5 g to 3.0 g per 100 mL, the gelation time decreases from $t_{gel} \geq 3000$ s to less than 10 s after 60 min mixing. However, because the extraction process involves unpurified natural ingredients, we observe large variations in t_{gel} for different samples with identical preparation, as shown in Supplementary Materials Fig. S1. The common qualitative features of the gelation process can be broken down into five distinct phases: (I) the pre-gel phase in which $G' < G''$ until G' increases sharply towards G''; (II) the gel point t_{gel} (taken here for simplicity as $G' = G''$) through which both G' and G'' rise sharply with time; (III) the loss modulus G'' passes through a local maximum followed by a minimum, after which G'' begins a final increase at a time we denote t^*(this time also corresponds to a concurrent inflection point in G' in many cases); (IV) the mature gel reaches the maximum storage modulus; (V) finally, at longer times the gel undergoes syneresis during which both G' and G'' slowly decline at long times.

The time evolution of the viscoelastic moduli of a set of extracts prepared in the same way all exhibit self-similarity when the evolution

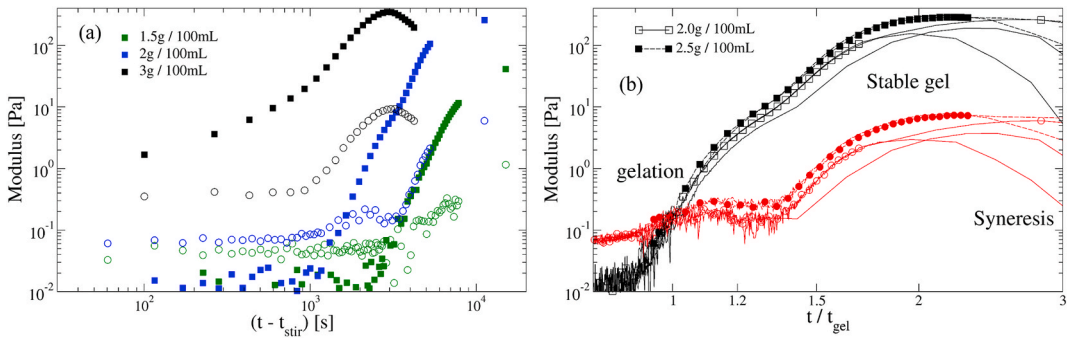

Fig. 2. The storage moduli (filled squares) and the loss moduli (hollow circles) for (a) time sweep at 10 rad/s, strain $\gamma_0 = 0.01$, for aiyu extract concentrations of 1.5 g (green), 2.0 g (blue), and 3.0 g (black) per 100 mL DI water. (b) Several independent measurements in which time is rescaled by t_{gel} for 2.0 g/100 mL (solid lines) and 2.5 g/100 mL (dashed lines) more clearly illustrating the characteristic phases in the evolution of the storage (black) and loss (red) moduli of several repeated measurements. (For interpretation of the references to colour in this figure legend, the reader is referred to the Web version of this article.)

time is referenced to t_{gel}, as shown in Fig. 2b. In particular, the reduced time t^*/t_{gel} for both the storage and loss moduli become quantitatively similar across many individual samples, as shown in Fig. S1 in Supplementary Materials. The sample-to-sample variations in t_{gel}, along with the consistent trends in the evolution observed with reduced time t^*/t_{gel}, support a model of two successive kinetic processes – with the later process dependent on the products of the earlier process. From previous literature (Durand et al., 1990; Huang et al., 1980), we identify the early process as the enzymatic activation of binding sites and the subsequent gelation process as the calcium to pectin binding. Fig. S1 also shows that t_{gel} and t^* possess a distinct correlation when we rescale the experiment time by t_{gel} for different seed weights, and for variations in the concentration of [NaCl], and [$CaCl_2$], which indicates that crosslink formation (from pectin calcium binding) is dependent on the enzymatic activation process.

In the early stages of the gelation process, intermolecular crosslinks gradually form, corresponding to the increase in G' as the network percolates the entire sample volume. The number of elastically-active segments (EAS), i.e. the number of segments between intermolecular crosslinks, is directly proportional to the number of crosslinks and reflected in the growth of the elastic modulus. As the crosslinked network forms, both G' and G'' increase with time, as is typical of many gelling systems; however, the observation of a local minimum and maximum in G'' with a corresponding inflection in G' is unusual and previously unreported to our knowledge. As the gelation process involves calcium binding to enzyme-activated PGA binding sites, we hypothesize that this distinctive inflection may be due to a progressive change in the characteristics of the crosslink distribution, i.e. a transformation of bound segments from shorter transient intermolecular associations to stronger and more long-lived junction zones (JZ) consisting of consecutively bound crosslinks.

As the initial seed concentration increases from 2 to 5 g/100 mL, the extracted PGA and ion concentrations also increase linearly. The averaged values for both t_{gel} and t^* decrease as the seed concentration increases, as shown in Fig. S1. We also find that the delay time $\Delta t^* = t^* - t_{gel}$ between crosslink re-arrangement remains nearly constant between 2000 and 3000 s, while t^*/t_{gel} increases from $t^*/t_{gel} = 1.3$ to $t^*/t_{gel} = 1.6$ as the seed concentration increases. This indicates that the transition to a stiffer network is dominated by junction zone (JZ) crosslinks, which depend on chain segment re-arrangements and calcium unbinding/rebinding, and is weakly dependent on the seed concentration. A plausible explanation is that the re-organization of crosslinks, given that the ratio of binders (calcium) and binding sites is independent of concentration, takes roughly the same amount of elapsed time for all seed concentrations studied. However, the initial gelation event (and thus t_{gel}) decreases with increasing seed concentration, the normalized "re-organization time" t^*/t_{gel} thus increases with increasing seed concentration.

Finally, although we observe gel syneresis at long times, both visually and in the measurements of the viscoelastic moduli, the total elapsed times at which syneresis occurs are not always consistent with each other. In several samples, the elastic modulus of the gel remained close to its maximum value long after the gel visually exuded a significant amount of water. This discrepancy may be due to how the gel adheres to the test fixture surfaces. Although these complications may be overcome with different surface treatments or test geometries, we do not systematically investigate gel syneresis in this study.

3.2. OWCh results

The frequency dependences of the viscoelastic moduli during gelation are computed from the resulting stress response to the windowed exponential chirp. Fig. 3a shows that G' increases and G'' decreases as the frequency ω increases from 0.3 to 10 rad/s. The inflection point in G' appears unchanged with frequency, while the plateau in G'' becomes lower and flatter as ω increases. To compactly characterize the material response, we consider a fractional Maxwell model for critical gels as in previous works (Geri et al., 2018; Jaishankar & McKinley, 2013; Koeller, 1984). For a slowly time-evolving linear viscoelastic system, the modulus can be written as

$$G(t;t^{'}-t) = \frac{\mathbb{G}(t)}{\Gamma[1-\alpha(t)]}(t'-t)^{-\alpha(t)} \tag{1a}$$

Or, equivalently, by taking a Fourier transform of this expression and assuming the rate of change in $\alpha(t)$ is small (i.e. the mutation number of the material is very small), we obtain the following expression for the real and imaginary parts of the complex moduli:

$$\begin{aligned} G^{'}(\omega,t) &= \mathbb{G}(t)\omega^{\alpha(t)}\cos\left(\alpha\pi/2\right) \\ G''(\omega,t) &= \mathbb{G}(t)\omega^{\alpha(t)}\sin\left(\alpha\pi/2\right) \end{aligned} \tag{1b}$$

In Eq. (1a), $G(t;t^{'}-t)$ is the relaxation modulus of the slowly aging gel at an arbitrary time and the time increment ($t^{'}-t$ for $t^{'} > t$ and $(t^{'}-t)/t_{gel} \ll 1$) represents the elapsed time following an imposed loading event at time t. Here $\Gamma(s)$ is the Gamma function of s. The expressions in Eq. (1) allow us to verify the fractional power law dependence of the gel through either step strain experiments or rapid frequency sweeps performed over short durations compared to the rate at which the gel is evolving or mutating. In Eq. (1), $\mathbb{G}(t)$ is the frequency-independent quasi-property characterizing the 'gel strength' (Jaishankar & McKinley, 2013) at time t, with units of Pa·s^{α}. The gel strength can be also found from measurements of the elastic and storage modulus at a time t by combining the expansions in Eq. (1b) to give

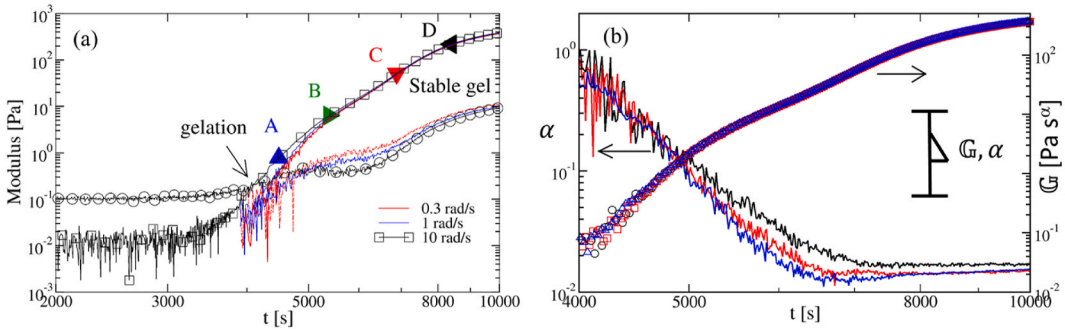

Fig. 3. (a) Evolution of the time-evolving storage modulus (squares) and loss modulus (circles) measured at $\omega = 0.3$ (red), 1.0 (blue), and 10.0 (black) rad/s for aiyu extracted with DI water at a concentration of 3.0g/100mL (stirred at 1400 rpm for 30 min). The triangles correspond to the selected times for the frequency sweeps shown in Fig. 4. (b) Evolution in the exponent (α) and the gel strength ($\mathbb{G}$) with time for the fractional spring-pot model (shown schematically in the inset). (For interpretation of the references to colour in this figure legend, the reader is referred to the Web version of this article.)

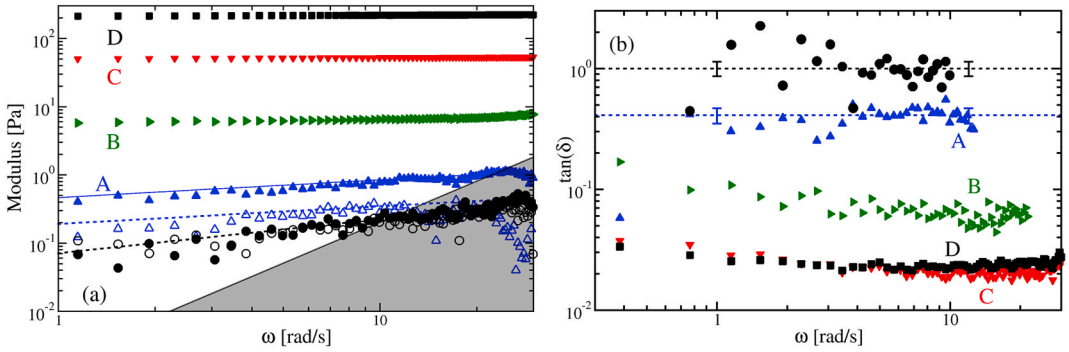

Fig. 4. Evolution in the linear viscoelasticity of aiyu gel extracted with DI water containing 3.0 g/100 mL seeds stirred at 1400 rpm for 30 min ($t_{gel} \approx 4100$ s). (a) Frequency sweeps showing the time evolution in the dynamic moduli. (a), with G′ (filled symbols) and G″ (hollow symbols) for $t = 4233$ s (black circles), 4500 s (blue triangles), 5400 s (green right triangles), 6900 s (red down triangles), and 8400 (black squares) s after 30 min mixing (from bottom to top). The grey region indicates the sample inertia limit, below which the oscillatory measurements are not reliable. The black dashed line at $t = 4233$ s corresponds to the prediction of Eq. (1b) with $\alpha = 0.49$ and $\mathbb{G}(t) \approx 0.1$ Pa·s^{α}. The blue solid and dashed lines at $t = 4500$ s correspond to Eq. (1b) with $\alpha = 0.26$ and $\mathbb{G}(t) \approx 0.5$ Pa·s^{α}. (b) Evolution in tan(δ) for the same data set, with data points that lie below the sample inertia limit removed. The black dashed line shows log (tan ($\delta(t = 4233$ s))) $= 0.00 \pm 0.14$, and the blue dashed line shows log(tan($\delta(t_A)$)) $= -0.38 \pm 0.06$, each averaged over $1.0 < \omega < 12.0$ rad/s. The standard deviations are shown as bars. (For interpretation of the references to colour in this figure legend, the reader is referred to the Web version of this article.)

$$\mathbb{G}(t) = \frac{\sqrt{(G'(\omega,t))^2 + (G''(\omega,t))^2}}{\omega^{\alpha(t)}} \tag{2}$$

The power law exponent $\alpha(t)$ captures the weak frequency dependence of the gel at time t and can be conveniently obtained from the phase angle

$$\tan(\delta(t)) = \frac{G''(\omega,t)}{G'(\omega,t)} \quad and \quad \alpha(t) = \frac{2}{\pi}\delta(t) \tag{3}$$

Fig. 3b shows that the evolution in $\mathbb{G}(t)$ is indeed frequency independent, indicating that the simple two-parameter model described by Eq. (1) adequately captures, in a compact way, both the power law frequency dependence and the time-evolving strength of this slowly evolving gel.

The power-law exponent of the growing network decreases from $\alpha \approx 0.5$ near t_{gel} and reaches a steady value $0.02 \leq \alpha \leq 0.03$ for $t > 7500$ s. The inflection point in $G'(\omega, t)$ is also distinctly observable in the evolution of the quasi property, or gel strength, $\mathbb{G}(t)$ at $t \approx 6000$ s. This is consistent with the observed physical process — the washed extract is a viscoelastic polymeric solution in the beginning and progressively transforms into a loosely connected hydrogel that then progressively stiffens over time. Fig. 3b shows the evolution of $\alpha(t)$ computed from measurements at $\omega = 1.0$, 3.8, and 10 rad/s. The curves all appear to cross near the gel point, within small fluctuations due to noise in the small values of the complex modulus at short times.

To further investigate the frequency dependence of the modulus with time, we choose four time points indicated by the triangles in Fig. 3a. We consider the instantaneous viscoelastic properties at $t = 4233$, 4500, 5400, 6900, and 8400 s obtained using an optimally windowed chirp (which takes only an elapsed test time $\Delta t_{chirp} = 15$ s, with $\Delta t_{chirp} \ll t_{gel}$). As shown in Fig. 4a, the elastic modulus $G'(\omega, t)$ increases by more than 100-fold as the gelation process evolves from $t_A = 4500$ to $t_D = 8400$ s, while the loss modulus G'' also increases by more than 10-fold. In the early stage of gelation (within 600 s after the crossover time which we use to identity $t_{gel} \approx 4100$ s), both G' and G'' still show a clear frequency dependence. After 1 h, as the gel network reaches maximum strength, G' becomes nearly independent of ω, and G'' now decreases slowly with increasing frequency. At $t = 4233$ s (near t_{gel}), Fig. 4b shows that the average value of the phase angle is tan(δ) ≈ 0.97, corresponding to $\delta = 0.77$ and $\alpha = 0.49$. We can also apply Eq. (1b) to find good agreement between the measured modulus over a wide range of oscillatory frequencies (as shown by the black line in Fig. 4a), which is consistent with critical gel theory (Winter & Chambon, 1986).

For $t_A = 4500$ s, the average value of the phase angle has dropped to tan(δ) ≈ 0.41 because G' grows more rapidly than G'' for $t > t_{gel}$ in Stage II. We thus find that $\alpha(t_A) = (2/\pi)\,\delta = 0.26$. By applying Eq. (1b), we find that the two parameter fractional viscoelasticity model again nicely captures the measured frequency dependence of $G'(\omega, t_A)$ and $G''(\omega, t_A)$ with a fitted value for $\mathbb{G}(t_A) \approx 0.5$ Pa·s^{α} as shown in Fig. 4a by the blue line. This agrees well with the estimated value for $\mathbb{G}(t_A) \approx 0.55$ Pa·s^{α} in Fig. 3b. Near $t_A = 4500$ s, tan(δ) also remains nearly constant for $0.6 < \omega < 10$ rad/s. By comparison, at longer times, tan(δ) decreases weakly

with frequency. The progressive flattening of the curves and the weak power-law slopes evident in Fig. 4a indicate a steady increase in the dominant relaxation time of the gelling system, which is characteristic of a soft glassy response (Winter 2013).

The evolution of the frequency exponent α from $\alpha \approx 0.5$ near the gel point to $\alpha(t_{gel}) \sim$ O (0.01) at longer times illustrates the steady evolution of the fractal structure of the network and the corresponding mechanical properties. Near the gel point the fractal dimension of a critical gel, as discussed by Muthukumar and Winter (Muthukumar & Winter 1986), can be computed to be $d_s = 2\ (1/\alpha - 1) = 2$ for $\alpha = 0.5$. The OWCh measurements provide a previously unattainable frequency spectroscopy of the slow transition in the aiyu jelly from a viscous fluid to an elastic network and some insights into the slowly evolving fractal nature of the gel network as it develops.

3.3. Microscopy

We performed time-synchronized cryo-scanning electron microscopy (cryo-SEM) with our rheological measurements throughout the gelation process. An aliquot of the gel extract was set aside as the remainder was loaded into the rheometer, and droplets from this sample were frozen and then sublimated at selected times just before (A) t_{gel}, (B) near t^*, and (C) at long times corresponding to the fully developed gel, as indicated by the dashed lines in Fig. 5a. As shown in Fig. 5b, a highly porous network formed before the gelation point (A). The pore sizes range from hundreds of nanometers to microns. The pores appear to be bounded by thin fibrous sheets with sheet width w_{sheet} of tens of microns and thickness of hundreds of nanometers. The higher magnification image shows populations of locally well-formed pores with large gaps in which short, thin fibers with width of a few hundred nanometers (Region I) are mixed with fibrous sheet-like walls (Region II). These structures are very similar to the fibrous networks observed in LM pectin gels (Kyomugasho et al., 2016). As the gelation progresses to near the inflection time t^* (B), we observe loose meshes of stiff nano-fibers that are tens of microns long. As the gel matures (C), fine fibrous networks with sub-micron mesh size are observed. As expected, the network mesh size of the polymer network steadily decreases as gelation progresses and the storage modulus steadily increases.

3.4. Effect of salt addition on gelation dynamics

Based on previous chemical analyses (Suzuno et al., 1997), the two most common inorganic species in aiyu extract are potassium (5.2 g per 100 g of dry matter) and calcium (0.95 g per 100 g of dry matter). For aiyu extract prepared from 2g seeds in 100 mL DI water, we obtain 0.15 g of dry matter as shown in Fig. 1b. We thus estimate that there are approximately 2.0 mM of K, 0.36 mM of Ca, along with trace amounts of Na in the extracted material. The high concentrations of monovalent ions such as K^+ found in the aiyu extract can bind with the acid side groups but cannot form crosslinks. Furthermore, intermolecular electrostatic interactions are modulated by the solvent ionic strength. Measurements show that in solutions with large amounts of monovalent

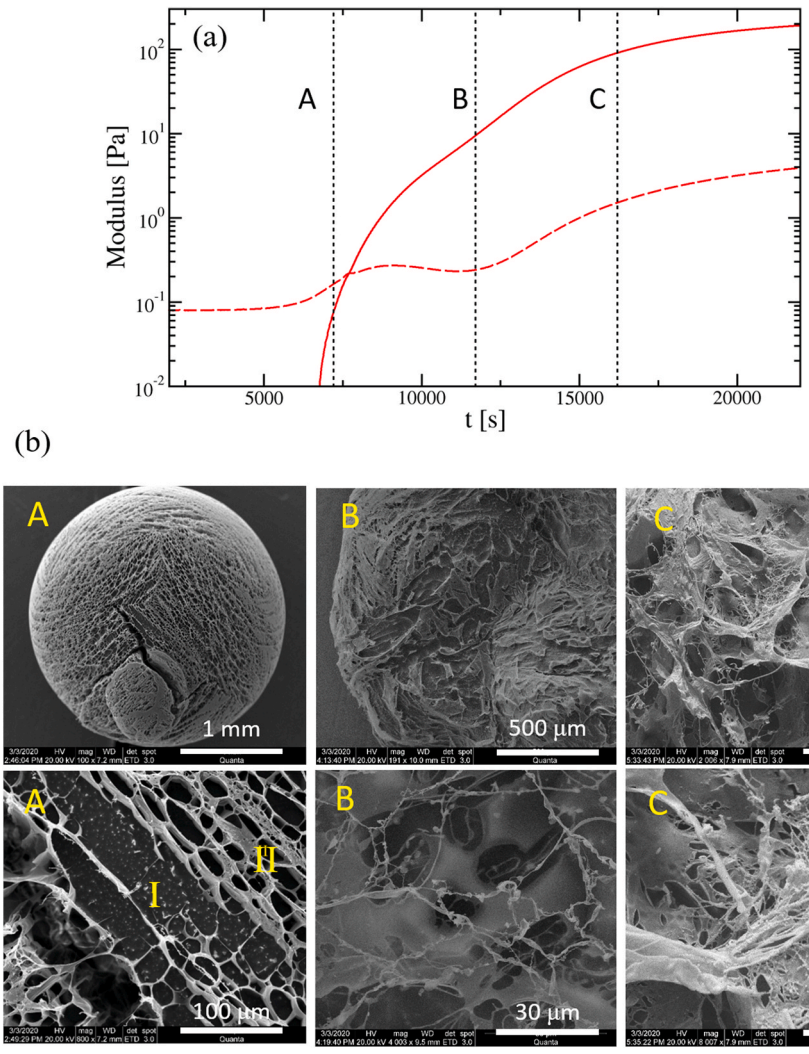

Fig. 5. Cryo-SEM images of aiyu jelly (2.0 g/100 ml) during the gelation process after 60 min mixing. (a) Evolution of the loss modulus (red dashed line) and the storage modulus (red solid line) with time at a frequency of ω = 10 rad/s. The dotted lines indicate the time at which the imaged samples are frozen; (b) cryo-SEM microscopy images with low (top) and high (bottom) resolutions at (A) 90 min, (B) 165 min, and (C) 240 min. (For interpretation of the references to colour in this figure legend, the reader is referred to the Web version of this article.)

ions, only around 50 percent of stoichiometric Ca^{2+} are strongly bound to PGA at equilibrium in the pectin-calcium system (Morris et al., 1982), and a similar ratio is expected for aiyu gels.

We also consider the effect of adding NaCl with concentrations up to 0.2 M to the aiyu extract. We expect [NaCl] addition will increase the ionic strength, reduce the electrostatic screening length and thus reduce inter-PGA electrostatic repulsion. Furthermore, enzyme activity may be inhibited at high ion concentrations (Huang et al., 1980). In addition, monovalent Na^{+} competes with Ca^{2+} for binding sites even though the monovalent ions cannot form crosslinks. Thus, the effect of increasing [NaCl] on t_{gel} and t^* is not clear, as shown in Fig. S1b. However, the delay time (t^*-t_{gel}) and the ratio t^*/t_{gel} consistently decrease as the monovalent ion concentration increases. This is consistent with the assertion that weaker inter-chain electrostatic repulsion results in increased likelihood for contacts between polymer segments, thus increasing binding between neighboring segments to form junction zones and larger aggregates, such as the sheet-like structures and elongated fibers observed with cryo-SEM in Fig. 5.

We also investigate through $CaCl_2$ addition how increasing the concentration of calcium ions affects gelation. As shown in Fig. S1c, we find t_{gel} and t^* decrease slightly upon increasing the calcium concentration, which can be attributed to the increased availability of the calcium crosslinkers. The qualitative characteristics observed in the time-evolving viscoelastic moduli are similar upon increasing [$CaCl_2$] from 0 to 4 mM in DI water during aiyu extraction. All PGA binding sites become occupied upon reaching the theoretical maximum binding ratio given by 2 [Ca^{2+}]/C_{GA} = 1. The GA concentration can be calculated to be $C_{GA} \approx 4.5$ mM for a seed concentration of 2 g/100 mL, as determined from the estimated PGA weight fraction (60%) of the total dry weight (Suzuno et al., 1997) (corresponding to ≈ 0.15 g/100 mL, from Fig. 1b) and the GA molecular weight of 194 g/mol. Thus, the theoretical calcium concentration at which all binding sites are crosslinked is expected to be [Ca^{2+}] ≈ 2.3 mM.

Fig. S1c shows that t^*/t_{gel} increases as the molar concentration of calcium is increased up to [Ca^{2+}] ≈ 2 mM, then t^*/t_{gel} decreases for [Ca^{2+}] = 3 and 4 mM. This non-monotonic variation may be attributed to how calcium addition affects the early enzymatic conversion process differently than the later junction zone re-organization process. From Fig. S1c, we find that the average value of t_{gel} decreases significantly as the calcium concentration increases up to [Ca^{2+}] ≈ 2 mM, followed by very little subsequent change with further increase in [Ca^{2+}]. This may indicate a couple of possible mechanisms, including the inhibition of enzyme activity at high [Ca^{2+}] and also a decreased binding rate due to increased electrostatic screening. We also find the crosslink rearrangement delay time (t^*-t_{gel}) decreases upon increasing calcium concentration, which indicates the microstructural transformation to a junction zone crosslinked network becomes accelerated with increased availability of calcium ions. The combined influences of calcium on these two processes contribute to the experimentally observed variations of t^*/t_{gel}.

4. Discussion

Our observations raise many interesting questions about aiyu gelation. For the same seed concentration, variations in the measured dry weights of the extracts are much smaller than the large sample-to-sample variations in t_{gel} and t^*, while the reduced or re-scaled time t^*/t_{gel} exhibits much smaller variance. Could the source of this variation be solely attributed to variations in enzyme activity and the initial degree of methoxylation? Here, we attempt to model the broad features of the gelation process using a simple reaction kinetics system combined with elementary elastic network theory.

We first estimate the aiyu extract viscosity and gel elasticity based on the observed parameters. We use the intrinsic viscosity estimated from the PGA molecular weight, $[\eta] = 3.28$ L/g, and the dry weight of 0.15 g/100 mL for a seed concentration of 2 g/100 mL to estimate the initial value of the loss modulus G'' in the sol. The linear relationship $G'' = \omega\eta$ connects the viscosity with the loss modulus, given by

$$G'' = \omega\eta \approx \omega\eta_s\left(1 + [\eta]\ C_p\right) \tag{4}$$

where the solvent viscosity $\eta_s = 10^{-3}$ kg/m s, $\omega = 10$ rad/s is the oscillatory frequency, and $C_p \approx 0.80$ g/L is the PGA weight concentration (60% of the total dry matter mass). Eq. (4) gives $G''\approx 0.0058$ Pa, which is in reasonable agreement with the measured value for the pre-gel extract liquid shown in Fig. 2a.

A rough estimate of the magnitude of the storage modulus in the gel can be obtained from the number of potential crosslink bonds that can be formed, which depends on the concentration of galacturonic acid groups on the PGA and the concentration of calcium ions. We estimate the GA molecular concentration $C_{GA} = 1000C_p/M_{GA} \approx 4.5$ mol/m^3 $= 2.7\times10^{24}$ molecules/m^3 from the molecular weight of the GA repeat unit $M_{GA} =$ 194 g/mol and the amount extracted in the dry matter shown in Fig. 1b. We also estimate the calcium ion concentration to be [Ca^{2+}] ≈ 0.36 mM for a seed concentration of 2g seed/100 mL and the reported amount of [Ca^{2+}] ≈ 1 g/100 g in the dry matter (Suzuno et al., 1997). With [Ca^{2+}] $< 0.5\ C_{GA}$, calcium concentration is the limiting factor for the number of crosslinks.

If every calcium ion formed a crosslink across two galacturonic acid sites, we can expect an upper limit of the elasticity at fully random binding to be $G_N = n\ k_BT \approx 880$ Pa, where n is the number density of crosslinks with a thermal energy scale $k_BT = 4.1\times10^{-21}$ J (at $T = 298$ K). If we further consider that the stable crosslinks formed at longer times consist of consecutively bound segments and the estimated average length of the stable crosslinks that develop in the "egg-box model" is reported (Ventura et al., 2013) to be between 6 and 10, we may anticipate that the average distance between crosslinks will be larger than the value estimated above and the plateau modulus of the mature gel may be $G_N \sim$ O (100 Pa), which agrees well with the observed storage modulus.

We seek to understand the gel formation dynamics observed in the frequency chirp and time sweep measurements. For physical networks with constant bond breakage and reformation with a binding equilibrium constant K_{bind}, Hermans (Hermans, 1965) derived an expression for the network modulus $G_N = (k_BT/2f\ K_{bind})[(a/a_c)\ (2 - W_g) - 2)](a/a_c)\ W_g$, where f is the crosslink functionality, a is the binding fraction, $a_c = 1/f$ is the critical gelation fraction, and W_g is the weight fraction of the gel. This model anticipates that once the network percolates and becomes elastic at the critical binding fraction a_c, the density of elastically active segments increases proportional to $[(a/a_c)^2(2 - W_g) - 2(a/a_c)]$, which approaches zero at the gel point when $a = a_c$ and $W_g = 0$. This expression accurately captures the sharp onset of elasticity and the increasing values of the storage modulus with increasing crosslink density. However, this model does not predict an inflection point in the evolution of the storage modulus with time.

Previous studies of gelation in calcium-pectin systems have emphasized the importance of the slow formation of long, consecutively bonded junction zones (JZ) in network formation (Ngouemazong et al., 2012a, 2012b). To describe the observed inflections in the evolution of the complex modulus, we hypothesize that the aiyu gel network comprises of an early weak gel stage consisting of transient crosslinks between PGA binding sites that break and reform at rates that depend on the salt concentration and other factors, and a later mature stage with slower-forming but more stable junction zone crosslinks, as illustrated schematically in Fig. 6a. For simplicity, we assume that the observed values of the viscoelastic moduli linearly combine contributions from these different and coexisting crosslinked networks. Rubber network theory predicts that the modulus of the network should be proportional to the number of elastically active strands (EAS). For networks with fixed numbers of binding sites, the number of elastically active strands increases with the number of crosslink bindings. A local inflection or decrease in the evolution of viscoelastic modulus with time reflects some new mechanisms that retard the growth of the number of EAS or even

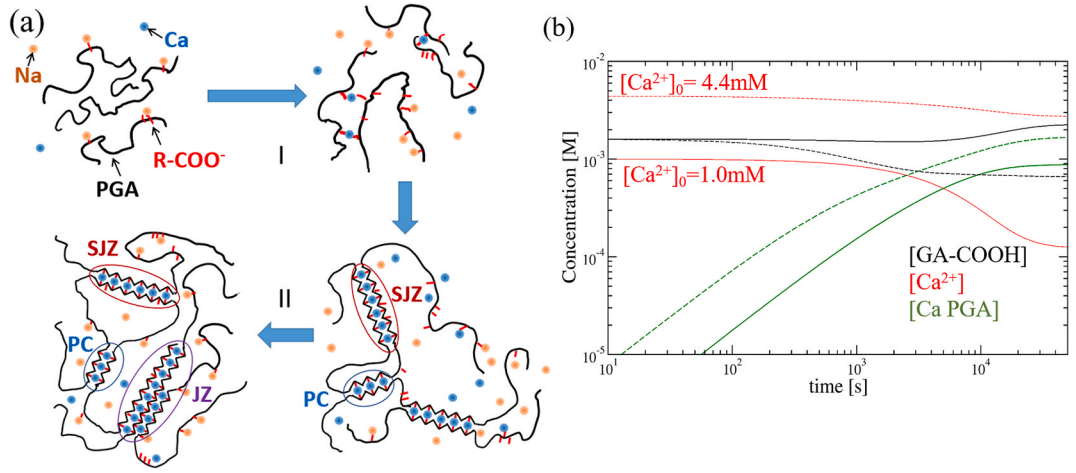

Fig. 6. (a) Illustration of our hypothetical model for (I) enzymatic reaction that activates binding sites and the initial binding events and (II) the slower structural transitions from shorter, consecutively bonded crosslinks to the longer and more strongly-bonded junction zones (JZ). The black lines show the PGA polymers, red lines indicate the activated binding sites (R-COO$^-$), blue spheres indicate calcium ions, and orange spheres indicate monovalent ions. (b) Model predictions with $k_1 = 70\ M^{-2}\ s^{-1}$, $k_{-1} = 5\times10^{-5}\ s^{-1}$, $k_{-1} = 1\times10^{-4}\ s^{-1}$, $[GA\text{-}COOH]_0 = 1.6$ mM, $[GA\text{-}COOCH_3]_0 = 2.4$ mM for seed concentration of 2 g/100 mL and $C_0 = 4.0$ mM. Evolution in the molarity of [GA-COOH] (black), $[Ca^{2+}]$ (red), and [Ca PGA] (green) in the sample with initial concentrations of $[Ca^{2+}]_0 = 1.0$ (solid line) and 4.4 (dashed line) mM respectively. (For interpretation of the references to colour in this figure legend, the reader is referred to the Web version of this article.)

decrease the number of EAS briefly. In an evolving system such as aiyu with an increasing number of total binding sites (which are being formed through enzymatic action), the growth of the number of EAS can plateau if new bonds are formed directly adjacent to existing bonded sites (to form a junction zone), and decreases if newly formed bonds merge two neighboring short JZs into one larger one. A transition from many weak reversible physical crosslinks into a smaller number of strongly crosslinked junction zones could thus account for the time-evolving trends observed in G' and G''. Here, we incorporate these elements into a reaction kinetics scheme and test whether our hypothesis can capture the observations.

4.1. Reaction kinetics

To describe the network formation kinetics in this system, we formulate a differential model for aiyu gelation kinetics. Past studies indicate pectin gelation follows (I) methylesterase enzyme transformation of methoxyl ester groups (-$COOCH_3$) to carboxyl groups (-COOH) along the backbone of polygalacturonic acids, (II) dissolved calcium ions bind to two carboxyl groups on the PGA backbone of two adjacent chains and form a transient physical crosslink, which is denoted as (Ca PGA). Thus,

$$GA\text{-}COOCH_3 + H_2O + E \xrightarrow{k_E} GA\text{-}COO^- + H^+ + CH_3OH + E \tag{5}$$

$$GA\text{-}COO^- + H^+ \overset{K_a}{\leftrightarrow} GA\text{-}COOH \tag{6}$$

$$Ca^{2+} + 2GA\text{-}COO^- \underset{k_{-1}}{\overset{k_1}{\leftrightarrows}} Ca\ PGA \tag{7}$$

Here E is the methylesterase enzyme concentration, k_E is the enzymatic rate constant, and K_a is the acid dissociation constant for carboxylic acid in water. We model the enzymatic reaction by Michaelis-Menten kinetics (Chaplin & Bucke, 1990). The calcium binding rate constant is k_1, and k_{-1} is the reverse reaction rate constant.

We observe that the pH value of aiyu extract remains nearly constant around pH ≈ 5 before gelation and after syneresis. We thus assume that the acid equilibrium does not change, and the dominant reactions are Eqs. (5) and (7). Thus, the time rate of change in the concentration of $GA\text{-}COOCH_3$ methoxylester and calcium ions are given by

$$\frac{d[GA\text{-}COOCH_3]}{dt} = \frac{-V_{max}[GA\text{-}COOCH_3]}{(K_m + [GA\text{-}COOCH_3])} \tag{8}$$

$$\frac{d[Ca]}{dt} = -k_1\gamma[Ca^{2+}][GA\text{-}COOH]^2 + k_{-1}[Ca\ PGA] \tag{9}$$

$$\frac{d[Ca\ PGA]}{dt} = k_1\gamma[Ca^{2+}][GA\text{-}COOH]^2 - k_{-1}[Ca\ PGA] \tag{10}$$

where $k_E = V_{max}/K_m = V_{max}{}^0/K_m\ [10^{\sqrt{I}}/(1+[H^+]/K_{e1} + K_{e2}/[H^+])] \approx 10^{-4}\ s^{-1}$ as reported in a previous measurement (Huang et al., 1980). Here V_{max} is the maximum enzymatic reaction rate, I is the ionic strength, and the enzymatic equilibrium constant is K_m. The two constants $K_{e1} \approx 10^{-3}$ M and $K_{e2} \approx 8.8\times10^{-10}$ M account for how pH affects enzyme activity and are obtained by fitting reported data in the literature (Huang et al., 1980; Jiang et al., 2001; Chaplin & Bucke, 1990). The coefficient γ in Eqs. (9) and (10) is the activity coefficient of calcium ions based on Debye-Huckel theory (Kielland, 1937) to take into account the effects of ionic strengths, given by

$$\log\gamma = \left(-0.51z_{Ca}^2\sqrt{I}\right)\Big/\left(1 + 3.3\beta_{Ca}\sqrt{I}\right) \tag{11}$$

where $I = \frac{1}{2}\sum[ion]z_{ion}^2$. Here z_{ion} is the ion valence and $\beta_{Ca} = 0.6$ nm is the effective diameter of the calcium ion.

For concentrations of the methylester group $[GA\text{-}COOCH_3] \ll K_m$, as is typical for the aiyu system, Eq. (8) is readily solved (Suzuno et al., 1997) by

$$[GA\text{-}COOCH_3] = C_{M0}\exp(-k_E\,t) \tag{12}$$

where $C_{M0} = [GA\text{-}COOCH_3]_0$ is the initial methyl ester group concentration, and $C_0 = C_{M0} + [GA\text{-}COOH]_0$ is the concentration of all possible binding sites. All other parameters can be derived from literature and are listed in the Supplementary Materials, Section II (Skoog et al., 2013).

To illustrate the solutions of Eqs. (8)–(10), we estimate that with a seed concentration of 2 g/100 mL, the total GA concentration is $C_0 \approx 4.0$ mM. Thus we calculate $[GA\text{-}COOCH_3]_0 = 2.4$ mM and $[GA\text{-}COOH]_0 = 1.6$ mM based on the reported degree of methylation ≈ 0.6 (Suzuno et al., 1997). As shown in Fig. 6b, the molecular concentrations of [GA-COOH] and $[Ca^{2+}]$ decrease with time and the concentration of [Ca PGA] increases, each reaching equilibrium concentrations at long times.

For a lower initial calcium ion concentration, $[Ca^{2+}] = 1.0$ mM, the carboxylic acid concentration [GA-COOH] increases with time after all $[Ca^{2+}]$ are bound, since the enzymatic reaction continues to convert GA-$COOCH_3$ to GA-COOH. The concentration of carboxylic acid [GA-COOH] becomes depleted only for sufficiently high calcium concentration $[Ca^{2+}]$ such that all available [GA-COOH] are bound. As further discussed in Supplementary Materials Section IV, the numerical solutions of Eqs. (8)–(10) show that the rate of change in the concentration of physical crosslinks d [Ca PGA]/dt and the maximum value of [Ca PGA] depend mainly on the rate constants k_1, k_{-1}, and k_E. By fitting the evolution in the storage modulus obtained from model predictions to that from the experimental observations, we can estimate these rate constants.

From Eqs. (10) and (12), we derive a single governing equation for the evolution in transient crosslink concentration [Ca PGA] given by

$$\frac{d[Ca\ PGA]}{dt} = k_1\gamma\left(\left[Ca^{2+}\right]_0 - [Ca\ PGA]\right)\left\{\left(C_0 - C_{M0}e^{-k_E t}\right) - 2[Ca\ PGA]\right\}^2 - (k_{-1})[Ca\ PGA] \tag{13}$$

where $[Ca^{2+}]_0$ is the initial calcium concentration. The determining factor for the number of bound sites is the binding ratio $R(t) = 2$ [Ca PGA]$/C_0$. Eq. (13) may be written in dimensionless form as

$$\frac{dR}{dt} = k_1 C_0^2\gamma(R_{max} - R)\left[1 - (C_{M0}/C_0)e^{-k_E t} - R\right]^2 - k_{-1}R \tag{14}$$

where the maximum binding ratio from stoichiometry is $R_{max} = 2$ $[Ca^{2+}]_0/C_0$.

4.2. Crosslink densities and the storage modulus

Based on previous measurements of the calcium and PGA content in dry matter (Suzuno et al., 1997), we estimate that $C_0 \approx 4.5$ mM and $[Ca^{2+}]_0 \approx 0.35$ mM for a seed concentration of 2g/100 mL in DI water extract. Approximately sixty percent of the initial PGA side groups are methyl esters, with $C_{M0} \approx 2.4$ mM (Huang et al., 1980). The proportion of consecutively bound sequences of length m is given by $p_m = R^{m-1}(1-R)^2$, where $R = R(t)$ is the instantaneous binding fraction that increases with time as more PGA sites are bound with calcium. Based on these estimates, $R_{max} = 2$ $[Ca^{2+}]_0/C_0 \approx 0.17$ in an extract of Aiyu jelly formed by washing in DI water alone without added salts.

The crosslink bonds can be distinguished into three categories by their physical characteristics, as illustrated in Fig. 7a. At the onset of gelation transiently bound point-like crosslinks (PC) form, with characteristic length $l < l_s$, and break with characteristic breakage rate that corresponds to the frequency-dependent peak in the loss moduli. This is followed by the formation of non-cooperative short junction zones (sJZ) with characteristic length l_s. In the mature gel, the stable junction zones (JZ) with characteristic length l_{JZ} form the major components of network crosslinks. We select $l_s = 6$ and $l_{JZ} = 8$ based on previously reported estimates (Ngouemazong et al., 2012b). Thus, the probability of finding a range of sequences of a given length in the range $m \in [m_1, m_2]$ is $P(t; m \in [m_1, m_2]) = \sum_{m_1}^{m_2} p_m = (1-R)\left(R^{m_1-1} - R^{m_2}\right)$. Furthermore, to connect the crosslink species concentration with the viscoelastic moduli, we hypothesize that the transition from sJZ to JZ is reflected by the inflection point in the storage modulus observed in the local minimum of the loss modulus observed in our experiments. The elastically active segments between the sJZ and JZ crosslinks both contribute (additively) to the measured overall elasticity of the network. The fractions of bound sites in each category are respectively given by (with detailed derivation given in Supplementary Materials Section III)

$$a_s JZ(R) = \sum_{m=l_s}^{l_{JZ}-1} m p_m = (1-R)\left[l_s R^{l_s-1} - l_{JZ}R^{l_{JZ}-1}\right] + R^{l_s} - R^{l_{JZ}} \text{ for } l_s \le l < l_{JZ}\ (\text{sJZ}) \tag{15}$$

$$a_{JZ}(R) = \sum_{m=l_{JZ}}^{\infty} m p_m = l_{JZ}R^{l_{JZ}}(1-R) + R^{l_{JZ}} \text{ for } l_{JZ} \le l\ (\text{JZ}) \tag{16}$$

With a random distribution of binding sites, the computed probabilities for consecutively bound sites with $R_{max} = 0.17$ are too small for the long junction zones (JZ) to become the dominant contribution to network elasticity, with $a_{JZ} \ll a_{sJZ}$ at all times as shown in Fig. 7b. From Eqs (15) and (16), we can estimate that the binding fraction needs to be $R \ge 0.8$ in order for $a_{JZ} > a_{sJZ}$ and for the JZ crosslinks to become the dominant contribution in the network.

However, the likelihood for successive [Ca PGA] bindings to be consecutive may be higher than expected for a completely random distribution. The spatial distribution of binding sites is in fact controlled by enzymatic conversion, the ionic interaction between the PGA chains, and the calcium ion concentrations. These factors have been probed in some details for the calcium pectin system (Ngouemazong et al., 2012a, 2012c). It has been reported that different methylesterase enzymes convert large blocks of *consecutive* binding sites with variations in the block length (Ngouemazong et al., 2012a). Thus, the probability of sequential calcium bindings and junction zone formation will be higher for block-distributed binding sites than for randomly distributed binding sites. For simplicity, we account for the higher likelihood of converted consecutive segments by an enzyme-enhanced sequential binding factor that we denote φ. The probability of crosslinks of type i is then given by $a_i(R(t)\varphi)$, where i indicates sJZ or JZ respectively. As shown in Fig. 7b, the fraction of consecutively bound [Ca PGA] junctions are significantly increased for $\varphi > 1$, such that the contribution of long and strong JZ crosslinks ($l \ge l_{JZ}$) grows to become more significant than short junction zone sJZ crosslinks ($l_{sJZ} \le l < l_{JZ}$) with time.

The number density of crosslinks of type i is $n_i(t) = C_0\, R(t)\, P(t; m \in [m_1, m_2])$ for $\varphi = 1$. With the enzyme-enhanced sequential binding factor $\varphi > 1$, we need to adjust the crosslink number density by the ratio

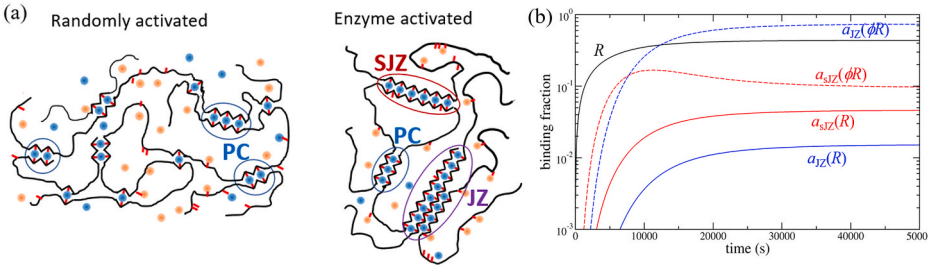

Fig. 7. (a) Illustration of binding site block length likelihood for randomly activated compared to enzyme activated binding sites. We select $6 \le l_{sJZ} < 8$ and $l_{JZ} \ge 8$ based on previous works (Durand et al., 1990; Ventura et al., 2013) Black lines show the PGA polymers, red lines indicate the activated binding sites (R-COO^-), blue spheres indicate calcium ions, and orange spheres indicate monovalent ions. (b) Evolution in the binding fractions with, and without, the enzyme factor φ. For $k_E = 10^{-4}$ s^{-1}, $k_1 = 70$ M^{-2} s^{-1}, $k_{-1} = 5{\cdot}10^{-5}$ s^{-1}, $[GA\text{-}COOCH_3]_0 = 2.4$ mM, $[GA\text{-}COOH]_0 = 1.6$ mM, for seed concentration of 2 g/100 mL and $C_0 = 4.0$ mM, with initial calcium ion concentration $[Ca^{2+}]_0 = 1.0$ mM. The black line shows the evolution of R with time, solid lines are for random-activated binding fractions $a_i(R)$ and dashed lines show the changes resulted from sequential enzyme-activated binding fraction $a_i(\varphi R)$ with $\varphi = 2$. Red lines show the initial evolution of the short junction zones (i = sJZ) and blue lines for the longer, more stable junction zones that develop at longer times (i = JZ). (For interpretation of the references to colour in this figure legend, the reader is referred to the Web version of this article.)

$[a_i(R(t)\varphi)/a_i(R(t))]$ such that $n_i(t) = C_0\ R(t)\ P(t; m \in [m_1, m_2])$ $[a_i(R(t)\varphi)/a_i(R(t))]$. As noted above, for simplicity, we consider the observed network modulus to be a linear superposition of contributions from the different types of crosslinked networks given by $G_N(t) \approx G_{sJZ}(t) + G_{JZ}(t)$. Furthermore, only the density of the elastically active segments ($n_i - n_{c,i}$) above the critical percolation threshold contributes to the total modulus, so that

$$G_N(t) = A(v/v_0)^{1/3} k_B T \sum_i (n_i(t) - n_{c,i}) \quad \text{for i} = \text{sJZ, JZ} \tag{17}$$

Here the unit transformation factor is denoted $A = 10^3\ N_A$ molecules•liter/(mol•m^3), v is the volume ratio of the polymer chains in the swollen gel and v_0 is the volume ratio of the polymer chains in the unswollen gel. The factor $(v/v_0)^{1/3}$ represents the average swelling length and accounts for the additional contribution to hydrogel elasticity due to the polymer swelling in the solvent (Rubinstein & Colby, 2003). The number of elastically active segments is estimated by the total number of crosslinks, including both sJZ and JZ types. We use the swelling ratio S, defined by $(v/v_0)^{1/3} \approx S\sum_i (n_i(t) - n_{c,i})/C_0$, to first fit the model to the measured maximum storage modulus. We find $n_{c,sJZ}$ determines the initial gel point, while $n_{c,JZ}$ determines the inflection point. How these two parameters affect the total modulus is discussed in the Supplementary Materials, Section V.

With the parameters given in Table 1, the model captures the observed evolution in the storage modulus for gelation of aiyu extract in DI water (2g aiyu seeds in 100 mL water) with added $CaCl_2$, as shown in Fig. 8a. The parameters $k_1 = 70\ M^{-2}s^{-1}$, $k_{-1} = 5\times10^{-5}\ s^{-1}$, $k_E = 10^{-4}\ s^{-1}$ are kept constant, consistent with our experimental observations that the change in [$CaCl_2$] only weakly affects the reaction rate constants. Rather than expressing the number density of crosslinks as defined in Eq (17) we convert this to the critical number of crosslinks per chain using the expression $N_{c,i} = N_p n_{c,i}/C_0$, considering that there are approximately $N_p \approx 10000$ maximum possible binding sites per chain, obtained by the ratio of the average polymer molecular weight ($\overline{M_w} \approx 2\times10^6$ g/mol) and the GA molecular weight. We note that as the calcium concentration increases, the enzyme-enhanced sequential binding factor φ decreases. As the calcium ion concentration increases, the binding fraction R also increases, and the differences between the likelihood of consecutively bound sites in random- and block-distributed gels decreases. In addition, we find that S decreases significantly at higher calcium concentrations. This may be attributed to an excess of calcium ions exhausting available GA binding sites, as we expect all binding sites are crosslinked at [Ca^{2+}] $\approx$ 2.3 mM, resulting in $S = 5$ for both [$CaCl_2$] = 2.0 and 4.0 mM. An excess of calcium ions may also facilitate junction zone formation, which is consistent with the decrease in $N_{c,JZ}$ for [$CaCl_2$] = 4.0 mM.

We also examine whether this reaction kinetics model captures how the gelation process varies with the initial seed concentration in DI water. As noted in our experimental observations, the sample-to-sample variations in t_{gel} and t^* are reduced when the experiment time is referenced to t_{gel}. We thus fit the model for a selected set of data with the total experiment time referenced to t_{gel} using the parameters given in Table 2. The influence of the washed seed concentration on the storage modulus evolution is captured by the model as shown in Fig. 8b. We estimate the initial concentration of all possible binding sites to be $C_0 = 3$, 4, 5, and 6 mM, corresponding to seed concentrations of 1.5, 2.0, 2.5, and 3.0 g/100 mL DI water, with a constant value of $C_{M0} = 0.6\ C_0$. Since the ratio of calcium ions to PGA is constant, we expect that the fraction of consecutive available binding sites and the swelling ratio remain the same as the seed weight increased, and we find $S \approx 200$ and $(v/v_0)^{1/3} \approx 4$ fits the measured modulus for most cases. Without $CaCl_2$ addition, we find both φ and S are higher than the values found for extracts with $CaCl_2$ addition, which is consistent with the trends observed in Table 1.

Table 1
Model parameters for fitting the experimentally observed dependence of the storage moduli dependence with increasing $CaCl_2$ concentration. Aiyu seed concentration of 2 g of seeds with 100 mL DI water and [$CaCl_2$] addition, stirred at 1400 rpm for 60 min.

Total Ca^{2+} [mM]	φ	S	$N_{c,sJZ}$	$N_{c,JZ}$
1.0	2	30	12	60
2.4	1.5	5	12	60
4.4	1	5	12	13

Table 2
Model parameters for fitting the experimentally observed dependence of the storage moduli to systematic changes of the concentration C_0 of all possible binding sites. Since we use a rescaled or dimensionless time t/t_{gel} to report and compare results, this also rescales the rate constants such that $k_1' = k_1\ t_{gel}$ and $k_E' = k_E\ t_{gel}$.

C_0 [mM]	t_{gel} [s]	φ	k_1' [M^{-2}]	k_E'	$N_{c,sJZ}$	$N_{c,JZ}$	S
3	6900	4.5	10^5	3	4	40	200
4	5200	4.5	10^5	3	17	40	200
5	4000	4.5	10^5	1.5	21	40	200
6	4090	4.5	10^5	0.5	10	40	180

As shown in Table 2, the onset gelation time t_{gel} decreases as the GA concentration C_0 increases, as expected. For $C_0 = 5$ and 6 mM, t_{gel} remains almost unchanged. By varying k_E and $N_{c,sJZ}$ the sharp onset of the growth in the gel storage modulus and the value of t^*/t_{gel} are captured for the different seed concentrations. This indicates that the network formation process is highly dependent on the enzymatic conversion rate k_E. In contrast, the critical number of JZ crosslinks ($N_{c,JZ} = 40$) per polymer is constant. Although we can note from Table 2 that k_1' is also constant, when we consider that the rescaled binding rate $k_1'(= k_1\ t_{gel})$ is referenced to t_{gel}, we note that the (dimensional) binding rate in fact increases with C_0. Although this is expected as higher PGA and calcium ion concentrations should increase the molecular collision likelihood and thus increase the rate of binding, it is not always clearly reflected in measurements of the gelation time t_{gel} due to the strong dependence of early reaction on enzymatic activity.

5. Conclusion

We have characterized the rheological and microstructural evolution of aiyu hydrogels during the gelation process. Aiyu jelly is a natural extract from *Ficus Pumila* var. *Awkeotsang* seeds that undergoes a pronounced sol – gel transition at room temperature with no added agents besides water. The rheological measurements at a single fixed frequency allow us to identify an interesting and previously unreported transient gelation phenomenon that is manifested as an inflection point in the evolving viscoelastic modulus $G^*(\omega, t)$ at intermediate times. We also employed rapid chirp-based sweeps to investigate the frequency dependence of the viscoelastic properties of the evolving gel for $0.3 < \omega < 30$ rad/s. Shortly after gelation, the storage modulus $G'(\omega, t \geq t_{gel})$ increases as a power law with frequency. The resulting power law exponent slowly decreases with time and the gel modulus gradually becomes frequency independent in the mature gel. In comparison, $G''(\omega, t \geq t_{gel})$ also initially increases as a power law with frequency. However, in the mature gel, the loss modulus decreases with frequency, signifying that the dominant relaxation time continuously increases as the gel matures. Comparison with a critical gel model shows that the fractional power law exponent monotonically decreases from $\alpha = 0.49$ close to gelation to approximately $\alpha \approx 0.02$ in the mature gel, indicating a loose microstructural arrangement with fractal dimension $d_f \approx 2$ near the gel point that subsequently evolves over a wide spectrum of length and time scales.

The microstructural evolution is also observed using cryo-SEM microscopy of the samples at different stages of the gelation process. We find the pectin fibers initially form fibrous meshes, with a mesh size decreasing from microns to hundreds of nanometers as the gel evolves,

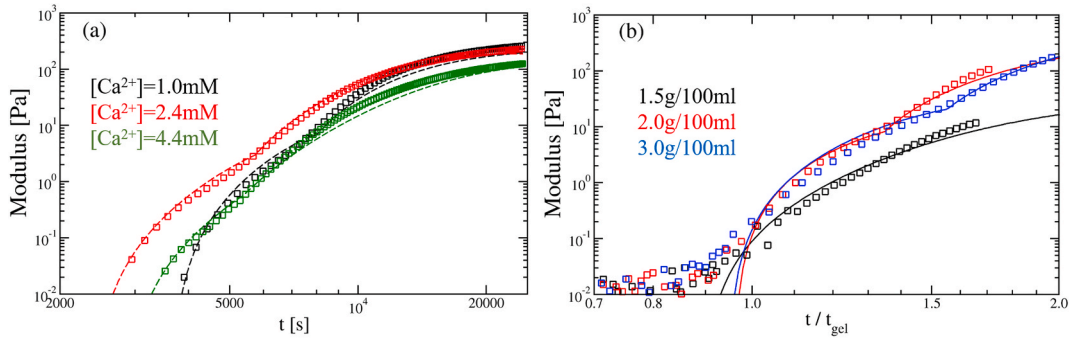

Fig. 8. Comparison between the time evolution of the predicted storage moduli (lines) at $\omega = 10$ rad/s and values measured in experiments (symbols). (a) Aiyu seed concentration of 2g of seeds with 100 mL DI water and [$CaCl_2$] addition, stirred at 1400 rpm for 60 min. Total concentrations of divalent calcium ions are $[Ca^{2+}]_0 =$ 1.0 (black), 2.4 (red), and 4.4 (green) mM. (b) Aiyu seed concentration of 1.5 (black), 2.0 (red), and 3.0 (blue) g/100 mL DI water, corresponding to initial concentration of all possible binding sites of $C_0 = 3$(black), 4(red), 6 (blue) mM, respectively. The model parameters are listed in Table1 and Table 2. (For interpretation of the references to colour in this figure legend, the reader is referred to the Web version of this article.)

with a corresponding increase in the network elasticity. The molecular origin of the gel network growth and evolution is expected to follow the proposed "egg-box" model for pectin-calcium gel networks, with the initial formation of transient point-like crosslinks and then consecutively bound junction zone "block" crosslinks with characteristic block lengths, as illustrated in Fig. 6.

Several studies on pectin-calcium gels formed with different methylesterase enzymes and gelation conditions have reported varying characteristic block lengths of the junction zone crosslinks. This led us to develop a quantitative model for the evolution in gel viscoelasticity by incorporating progressive microstructural transitions of the point-like transient crosslinks first to shorter, weaker JZs and eventually to longer, more tightly-bound JZs. By combining a simple reaction kinetics model with rubber network theory, our proposed model captures the viscoelasticity evolution during aiyu gelation. It includes the essential physical mechanisms – methylesterase enzyme-driven creation of binding sites, calcium-pectin binding and the formation of consecutively bound junction zone blocks, to capture the onset of elasticity once a critical number of elastically active segments are formed such that the growing network spans the sample volume. The model shows that these basic structural elements are sufficient to describe the physical process of aiyu gel formation, and the mechanisms embodied by this model can be generalized for other gelation systems in which binding sites are activated by enzymatic action.

Although the mechanisms embedded in the model are physically straightforward, there are numerous associated model parameters that need to be determined via careful measurement. Parameters such as the PGA molecular weight and concentration, the initial degree of methylation, and the ion concentrations in the aiyu extracts can be measured, and we have always used literature-reported values for our model computations. The enzyme reaction rate constant and the calcium binding/unbinding rate constants have also been previously measured, and our model also uses the reported estimated values. We thus reduce the key unknown parameters that the model requires in order to fit the observed elasticity evolution and distinct inflection point feature to (i) the enzyme-enhanced binding factor φ, (ii) the swelling factor S of the resulting hydrogel, and (iii) the critical concentrations $N_{c,\ sJZ}$ for the onset of network elasticity and $N_{c,\ JZ}$ for the inflection point. Future studies could employ computational models of polyelectrolyte binding with multivalent ions to better understand how binding site segment distribution, modified by specific enzyme action, affects junction zone formation. Microstructural (possibly lattice-based) modeling of an evolving crosslinking network would also provide additional physical insights into the critical criteria for emergence of network elasticity and the frequency dependence of the modulus evolution beyond the simple additive model proposed. With better physical understanding of pectin-based gelation mechanisms in natural biopolymers such as aiyu jelly, future studies could explore how to design synthetic self-gelling foods and custom-design biopolymers with tailored gelation profiles and gel strengths.

CRediT authorship contribution statement

Fan-Wei Wang: Conceptualization, Methodology, Investigation, Formal analysis, Writing – original draft. **Michela Geri:** Conceptualization, Methodology, Investigation, Formal analysis, Writing – review & editing. **Yun-Ju Chen:** Methodology, Investigation, Formal analysis, Writing – review & editing. **Jung-Ren Huang:** Methodology, Resources, Writing – review & editing. **Gareth H. McKinley:** Conceptualization, Formal analysis, Resources, Supervision, Writing – original draft. **Yeng-Long Chen:** Conceptualization, Investigation, Formal analysis, Resources, Supervision, Writing – original draft.

Declaration of competing interest

None.

Acknowledgements

We thank Dr. Bavand Keshavarz, Dr. Chia-Fu Chou, Dr. Chi-Keung Chan and Mr. Jing-Ting Chu for their assistance with the experiments, Ms. Crystal Owens for assistance with ion conductivity measurements and Mr. Sami Yamanidouzisorkhabi for assistance with Schlieren imaging. We also thank Dr. Shih-Lung Tu and the AS Institute of Plant Molecular Biology cryo-SEM imaging facility for their assistance. This work was supported by the Ministry of Science and Technology, Taiwan. MOST 107-2112-M-001-031-MY3 and 110-2918-I-001 -005.

Appendix A. Supplementary data

Supplementary data to this article can be found online at https://doi.org/10.1016/j.foodhyd.2021.107001.

References

Axelos, M. A. V., Lefebvre, J., & Thibault, J. F. (1987). Conformation of a low methoxyl citrus pectin in aqueous solution. *Food Hydrocolloids, 1*, 569.
Braccini, I., & Pérez, S. (2001). Molecular basis of Ca2+-induced gelation in alginates and pectins: The egg-box model revisited. *Biomacromolecules, 2*(4), 1089–1096.
Chan, S. Y., Choo, W. S., Young, D. J., & Loh, X. J. (2017). Pectin as a rheology modifier: Origin, structure, commercial production and rheology. *Carbohydrate Polymers, 161*, 118.
Chaplin, M. F., & Bucke, C. (1990). *Enzyme technology*. CUP Archive.
Durand, D., Bertrand, C., Clark, A., & Lips, A. (1990). Calcium-induced gelation of low methoxy pectin solutions—thermodynamic and rheological considerations. *International Journal of Biological Macromolecules, 12*(1), 14–18.

Garnier, C., Axelos, M. A. V., & Thibault, J. F. (1993). Phase diagrams of pectin-calcium systems: Influence of pH, ionic strength, and temperature on the gelation of pectins with different degrees of methylation. *Carbohydrate Research, 240*, 219.
Gawkowska, D., Cybulska, J., & Zdunek, A. (2018). Structure-related gelling of pectins and linking with other natural compounds: A review. *Polymers, 10*, 762.
Geri, M., Keshavarz, B., Divoux, T., Clasen, C., & McKinley, G. H. (2018). Time-resolved mechanical spectroscopy of soft materials via optimally windowed chirps. *Physical Review X, 8*, Article 041042.
Graessley, W. W. (1980). Polymer chain dimensions and the dependence of viscoelastic properties on concentration, molecular weight and solvent power. *Polymer, 21*(3), 258–262.
Grant, G. T., Morris, E. R., Rees, D. A., Smith, P. J. C., & Thom, D. (1973). Biological interactions between polysaccharides and divalent cations: The egg-box model. *FEBS Letters, 32*(1), 195.
Hermans, J. (1965). Investigation of the elastic properties of the particle network in gelled solutions of hydrocolloids. I. Carboxymethoyl cellulose. *J. Polym. Sci. Part. A, 3*, 1859.
Huang, Y. C., Chen, W. B., & Shao, Y. P. (1980). A study on the mechanism of gelatinization of awkeo-jelly. *J. Taiwan Soc. Horticultural Sci., 26*(5&6), 117–126.
Jaishankar, A., & McKinley, G. H. (2013). Power-law rheology in the bulk and at the interface: Quasi-properties and fractional constitutive equations. *Proc. R. Soc. A, 469*, 20120284.
Jiang, C. M., Lai, Y. J., Lee, B. H., Chang, W. H., & Chang, H. M. (2001). De-esterification and transacylation reactions of pectinesterase from jelly fig (Ficus awkeotsang makino) achenes. *Journal of Food Science, 66*(6), 810–815.
Kielland, J. (1937). Individual activity coefficients of ions in aqueous solutions. *Journal of the American Chemical Society, 59*(9), 1675–1678.
Koeller, R. C. (1984). Applications of fractional calculus to the theory of viscoelasticity. *Journal of Applied Mechanics-Transactions of the ASME, 51*(2), 299–307.
Kyomugasho, C., Christiaens, S., Van de Walle, D., Van Loey, A. M., Dewettinck, K., & Hendrickx, M. E. (2016). Evaluation of cation-facilitated pectin-gel properties: Cryo-SEM visualisation and rheological properties. *Food Hydrocolloids, 61*, 172–182.
Lu, M. C., Liu, Y. C., & Hsuan, C. L. (2019). Cultivation and environment of Taiwan endemic species jelly fig (Ficus awkeotsang makino). *Agr. Biotech. Industry Quarterly, 59*, 27.
Luzio, G. A., & Cameron, R. G. (2008). Demethylation of a model homogalacturonan with the salt-independent pectin methylesterase from citrus: Part II. Structure–function analysis. *Carbohydrate Polymers, 71*(2), 300–309.
Morris, E. R., Powell, D. A., Gidley, M. J., & Rees, D. A. (1982). Conformations and interactions of pectins I. Polymorphism between gel and solid states of calcium polyglacturonate. *Journal of Molecular Biology, 155*, 507.
Muthukumar, M., & Winter, H. H. (1986). Fractal dimension of a cross-linking polymer at the gel point. *Macromolecules, 19*, 1284.
Ngouemazong, D. E., Jolei, R. P., Cardinaels, R., Fraeye, I., Van Loey, A., Moldenaers, P., & Hendrickx, M. E. (2012b). Stiffness of Ca^{2+}-pectin gels: Combined effects of degree and pattern of methylesterification for various Ca^{2+} concentrations. *Carbohydrate Research, 348*, 69–76.
Ngouemazong, D. E., Nkemamin, N. F., Cardinaels, R., Jolie, R. P., Fraeye, I., Van Loey, A. M., Moldenaers, P., & Hendrickx, M. E. (2012c). Rheological properties of Ca^{2+}-gels of partially methylesterified polygalacturonic acid: Effect of "mixed" patterns of methylesterification. *Carbohydrate Polymers, 88*(1), 37–45.
Ngouemazong, D. E., Tengweh, F. F., Fraeye, I., Duvetter, T., Cardinaels, R., Van Loey, A., Moldenaers, P., & Hendrickx, M. E. (2012a). Effect of de-methylesterification on network development and nature of Ca^{2+}-pectin gels: Towards understanding structure-function relations of pectin. *Food Hydrocolloids, 26*(1), 89–98.
Oda, Y., & Tanaka, R. (1966). Studies on the polyuronide of oh-gyo-tye *agr*. *Biological Chemistry, 30*(4), 406.
Rubinstein, M., & Colby, R. H. (2003). *Polymer Physics. United States*. New York: Oxford University Press Inc.
Skoog, D. A., West, D. M., Holler, F. J., & Crouch, S. R. (2013). *Fundamentals of analytical chemistry*. Nelson Education.
Suzuno, H., Kinugasa, S., Nakahara, H., & Kawabata, A. (1997). Molecular Characteristics of water-soluble polysaccharide extracted from jelly fig (ficus awkeotsang Makino) seeds. *Bioscience Biotechnology & Biochemistry, 61*(9), 1491–1494.
Suzuno, H., Shen, F., Sawayama, S., & Kawabata, A. (1994). Weakness of aqueous polysaccharide gels prepared from jelly fig. *Journal of Home Economics of Japan, 45*(12), 1089–1094.
Suzuno, H., Uchibori, Y., & Sawayama, S. (1991). Rheological properties of aqueous polysaccharide sols and gels prepared from jelly fig. *Journal of Home Economics of Japan, 42*(12), 1043.
Urias-Orona, V., Rascon-Chu, A., Lizardi-Mendoza, J., Carvajal-Millan, E., Gardea, A. A., & Ramirez-Wong, B. (2010). A novel pectin material: Extraction, characterization and gelling properties. *International Journal of Molecular Sciences, 11*, 3686.
Ventura, I., Jammal, J., & Bianco-Peled, H. (2013). Insights into the nanostructure of low-methoxyl pectin-calcium gels. *Carbohydrate Polymers, 97*(2), 650–658.
Wang, R., Liang, R.-H., Dai, T., Chen, J., Shuai, X., & Liu, C.-M. (2019). Pectin-based adsorbents for heavy metal ions: A review. *Trends in Food Science & Technology, 91*, 319.
Winter, H. H. (2013). Glass transition as the rheological inverse of gelation. *Macromolecules, 46*(6), 2425–2432.
Winter, H. H., & Chambon, F. (1986). Analysis of linear viscoelasticity of a cross-linking polymer at the gel point. *Journal of Rheology, 30*(2), 367–382.
Wu, H. H., Wu, D. C., & Chia, C. Y. (2007). Studies on the factors influencing the quality and gelation of jelly fig (Ficus awkeotsang makino). *Bullet. Miaoli Dist. Agri. Res. Ext., 1*, 59.